Journal of Luminescence 132 (2012) 2385–2389

Contents lists available at SciVerse ScienceDirect

Journal of Luminescence

journal homepage: www.elsevier.com/locate/jlumin

Photoluminescence mechanisms in silicon quantum dots embedded in nanometric chlorinated-silicon nitride films

A. Rodriguez [a], J. Arenas [b], J.C. Alonso [a,*]

[a] Instituto de Investigaciones en Materiales, Universidad Nacional Autónoma de México. A. P. 70-360, Coyoacán 04510, D. F., Mexico
[b] Instituto de Física, Universidad Nacional Autónoma de México. A. P. 20-364, Coyoacán 01000, D. F., Mexico

ARTICLE INFO

Article history:
Received 28 November 2011
Received in revised form
28 February 2012
Accepted 4 April 2012
Available online 14 April 2012

Keywords:
Photoluminescence
Silicon
Quantum dots

ABSTRACT

Silicon quantum dots (Si-QDs) embedded in nanometric (~80 nm) chlorinated-silicon nitride films (SiN_x:Cl) were prepared by remote plasma enhanced chemical vapor deposition. The photoluminescence (PL) peak and the two optical absorption edges observed in the PL and absorption spectra of the films were tuned (blue-shifted) as the Si-QD size was decreased, giving evidence of quantum confinement effects. From these results we elucidate that the photoluminescence in these nanostructured films is generated by photoexcitation of electrons from the valence band tail of the SiN_x:Cl matrix toward the conduction band tail of the SiN_x:Cl matrix and the conduction band of the Si-QDs, followed by diffusion and transfer of electrons and holes from the SiN_x:Cl matrix to the Si-QDs, and then electron–hole radiative recombination in the Si-QDs. These PL mechanisms explain quite well the large absorption/emission Stokes shift that was experimentally observed in these films.

1. Introduction

Silicon quantum dots (Si-QDs) or nanocrystals (Si-nc) embedded in silicon oxide (SiO_x), silicon nitride (SiN_x) and silicon carbide (SiC) films, are being intensively investigated as light sources for the development of low-cost silicon-based photonic and optoelectronic devices [1–17]. Although visible photoluminescence (PL) at room temperature has been already obtained from many of these silicon-based nanostructured systems, the origin and properties of this PL are not completely understood at present. Some experimental works have shown that quantum confinement effects (QCE) of excitons in the Si-QDs play the most important role for obtaining and controlling their photoluminescence (PL) [7,8,10]. However, other experimental and theoretical works have shown that surface passivation and/or localized defects at the Si-QDs/dielectric matrix interface, have also strong influence on the PL properties of the Si-QDs [9,12,14,16–21]. On the other hand, in spite of the large absorption/emission Stokes shift that has been experimentally observed in silicon nitride films with Si-QDs, [11,12], the origin of this shift has not been explained and neither the mechanisms of excitation–emission of light in these nanostructured systems. In order to get more insights on the origin of this PL and to obtain it in an efficient and controlled manner, and since in practice the absorption–emission mechanisms depend on the specific nanostructured system, this topic continues being of great interest. In this work we provide experimental results which evidence QCEs in the tunable visible PL and absorption of Si-QDs embedded in nanometric chlorinated SiN_x films (SiN_x:Cl), and proposed a model to explain the mechanisms of excitation–emission of light in these nanostructured films.

2. Experimental

The films were deposited on n-type (1 0 0) silicon and fused silica substrates by remote plasma enhanced chemical vapor deposition using $SiH_2Cl_2/NH_3/H_2/Ar$ mixtures and the deposition system reported previously [15]. The substrate temperature, rf power, and total deposition pressure were fixed at 300 °C, 150 W, and 300 mTorr, respectively. The flow rates of the SiH_2Cl_2, H_2, and Ar gases were fixed at 5, 20, and 150 sccm, respectively. The series of samples investigated here were obtained using flow rates of NH_3 of 50, 100, 200, and 300 sccm. The deposition times were adjusted to obtain films with the same thickness of approximately 80 nm. This nanometric thickness was chosen for all the films in order to avoid the appearance of multiple peaks (by interference effects) in both, the photoluminescence and transmission spectra of thick films [11–13,15], which hinder the analysis of the main features of the spectra (PL peak, absorption edges, etc.) as a function of the Si-QD size. The thickness (Th) of the films was measured using a manual Gaertner 117 ellipsometer equipped with a He–Ne laser (λ=632 nm). A VG Microtech Multilab ESCA 2000 System was used to carry out X-ray photoelectron spectroscopy (XPS) to determine the N/Si ratio and Cl at%. Table 1 lists

* Corresponding author. Tel.: +55 52 56 22 46 06.
E-mail address: alonso@unam.mx (J.C. Alonso).

0022-2313/$ - see front matter © 2012 Elsevier B.V. All rights reserved.
http://dx.doi.org/10.1016/j.jlumin.2012.04.007

the N/Si ratios and Cl at% for the films investigated in this work. As this table shows, all the SiN_x:Cl films are silicon rich with respect to stoichiometric silicon nitride (Si_3N_4 or N/Si=1.33) and become less silicon rich (the N/Si ratio increases) as the NH_3 flow rate increases. Photoluminescence (PL) measurements were carried out in a dark room at room temperature, using an unfocused beam of 25 mW from a Kimmon He–Cd laser operating at 325 nm (3.81 eV). The PL spectra were recorded with a Fluoromax-Spex spectrofluorometer. Ultraviolet–visible (UV–vis) transmission measurements were carried out in the range from 300 to 1100 nm using a double-beam PerkinElmer Lambda 35 UV–vis spectrophotometer. The presence and size of the Si-QDs was confirmed by high resolution transmission electron microscopy (HRTEM) using a field emission gun (JEM-2010F) which operates at 200 kV near the Scherrer focus, with a theoretical point to point resolution of 0.19 nm. The HRTEM images in planar view samples were recorded with a CCD camera and treated with a digital analysis program. Mechanical grinding and ion milling processes were employed for the electron transparency thinning of the samples.

3. Results and discussion

Fig. 1(a)–(d) show some HRTEM images of Si-QDs embedded in silicon nitride films deposited at the different NH_3 flow rates. As can be seen qualitatively from these images, the Si-QD size decreases as the NH_3 flow rate increases, and this effect is consistent with the fact that the films become less rich in silicon. A careful analysis of several HRTEM images for each NH_3 flow rate was made in order to extract the approximate average size (d) and density per unit area (σ) of Si QDs with sizes up to 6 nm. As the histograms of Fig. 2 show, the distribution of sizes shift towards smaller sizes as the NH_3 flow rates. The values of d and σ are listed in Table 1. This table shows that d decreases as the NH_3 flow rates increases from 50 to 300 sccm, meanwhile σ first increases as the NH_3 flow rates increases up to 200 sccm, and then decreases for 300 sccm of NH_3. The HRTEM analysis also revealed that the SiN_x:Cl matrix is amorphous, and that the Si-QDs tend to be more crystalline as their size increases.

Fig. 3 shows the PL spectra obtained for the films deposited at the different NH_3 flow rates. The normalized PL intensity is also

Table 1
Empirical data of composition, PL and optical absorption characteristics, and QCE parameters of SiN_x:Cl thin film with Si-QDs embedded.

NH_3 flow rate (sccm)	N/Si ratio	Cl (at%)	PL peak (nm)	d (nm)	σ (#/cm^2)	$E_{PL}=E_g$ (eV)	$E_{edge1}=E_{gtail}$ (eV)	$E_{edge2}=E_{g'}$ (eV)	ΔE (eV)	C (nm^2 eV)
50	0.70	4.5	540	3.9	7.8×10^{11}	2.3	3.0	3.8	0.4	17.3
100	0.91	4.7	528	3.7	2.1×10^{12}	2.35	3.1	3.8	0.35	16.3
200	1.05	4.8	496	3.1	6.0×10^{12}	2.5	3.3	4.2	0.45	12.9
300	1.16	3.9	436	2.4	1.4×10^{12}	2.84	3.5	4.5	0.5	9.7

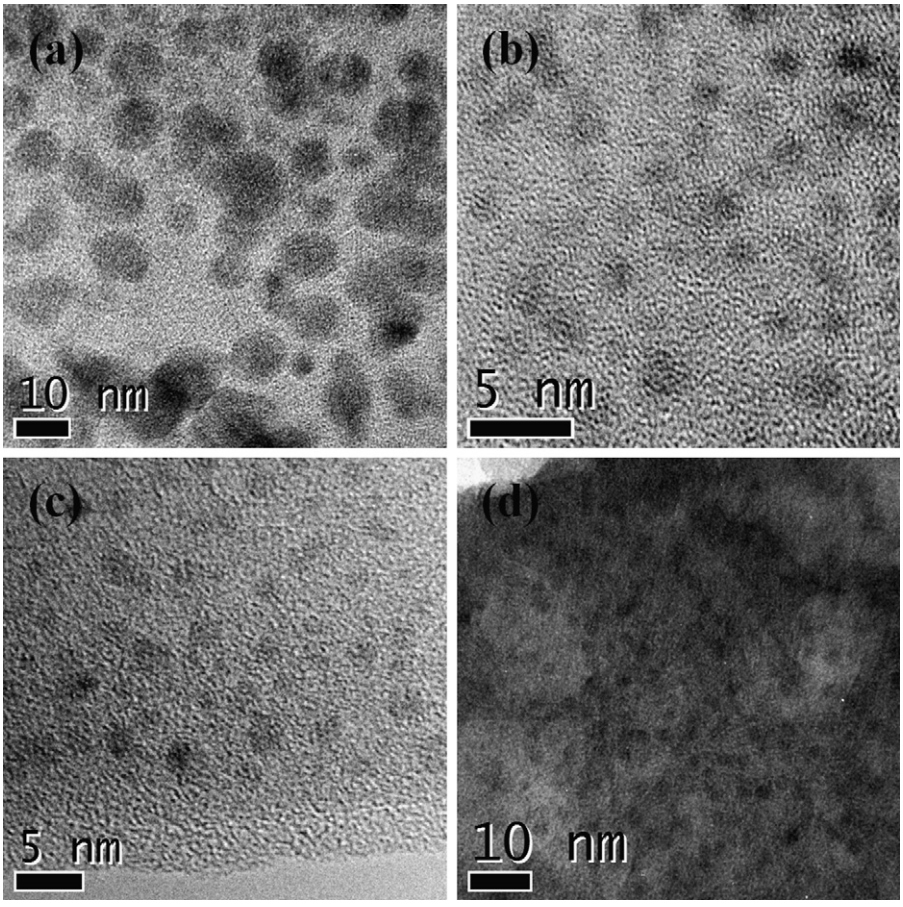

Fig. 1. HRTEM images showing Si-QDs embedded in a SiN_x:Cl films deposited with (a) 50 sccm, (b) 100 sccm, (c) 200 sccm and (d) 300 sccm of NH_3. The scale is 10 nm in (a) and (d), and 5 nm in (b) and (c).

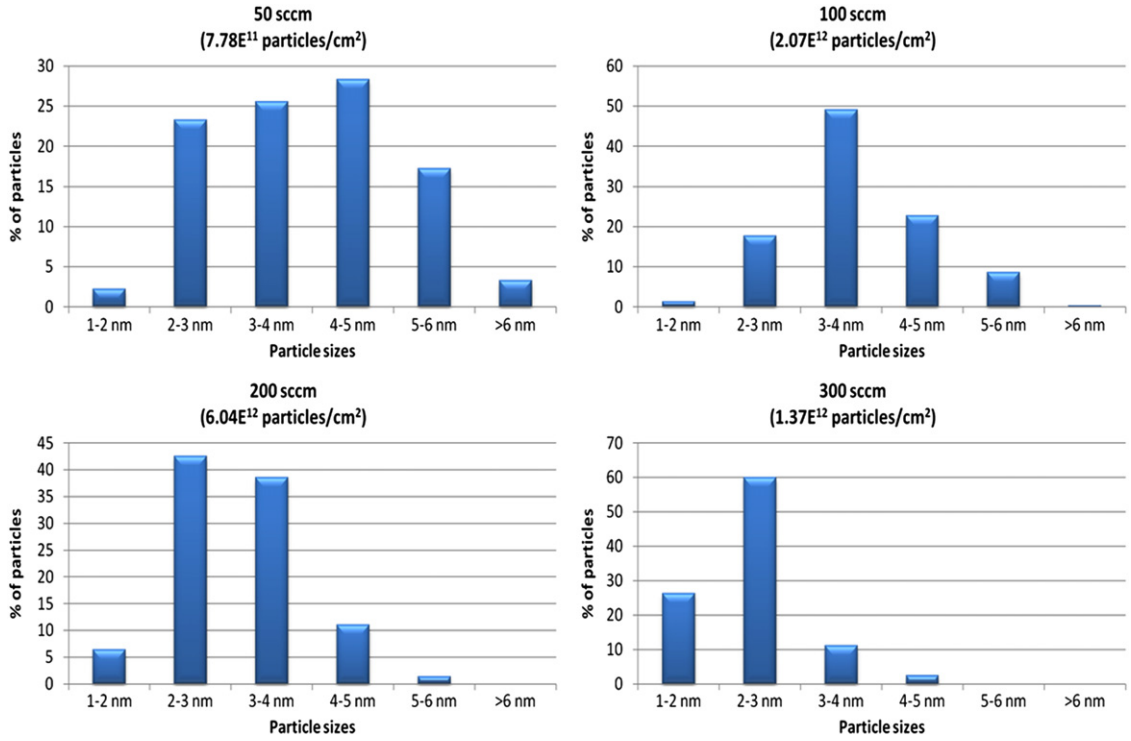

Fig. 2. Histograms of the size distribution and density of Si-QDs for the SiN_x:Cl films as a function of NH_3 flow rate.

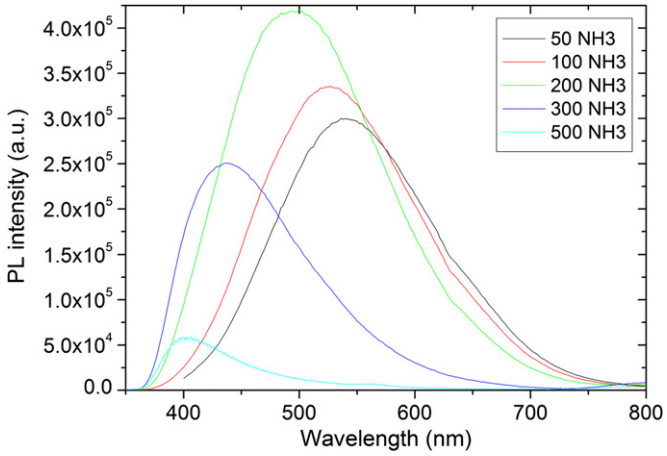

Fig. 3. PL emission spectra of SiN_x:Cl nanometric (~80 nm) films with Si-QDs deposited with NH_3 flow rates of 50 sccm (black), 100 sccm (red), 200 sccm (green), 300 sccm (blue) and 500 sccm (light blue). (For interpretation of the references to color in this figure legend, the reader is referred to the web version of this article.)

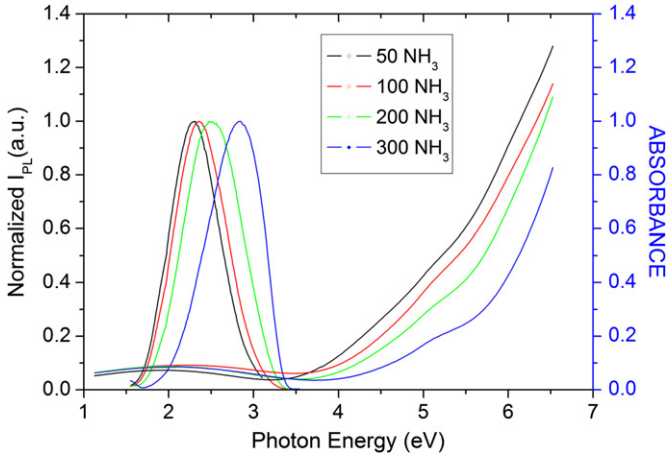

Fig. 4. Normalized PL and absorbance spectra as a function of photon energy for films deposited with different NH_3 flow rates.

plotted in Fig. 4 as a function of the photon energy. According to the quantum confinement effect (QCE) model, the major contribution to the luminescence of these films comes from radiative recombination of electron–hole pairs in the Si-QDs, and therefore the energies (E_{PL}) of the PL peaks, whose values are given in Table 1, can be directly associated with the band gap energy ($E_g = E_c - E_v$) of the Si-QDs [7,8,10,22]. As it can be seen from Figs. 3 and 4, the PL peak blue-shifts (shifts toward shorter wavelengths or higher energies) as the NH_3 flow rate increases. Since the Si-QD sizes decrease as the NH_3 flow rate increases, this blue-shift can be also explained in terms of the QCE model, which predicts that the Si-QDs band gap becomes quasi-direct and increases as the Si-QD size decreases below the Bohr radius of excitons in confined silicon (~5.3 nm) [22].

The changes in the PL intensity (Fig. 3) of the films with the NH_3 flow rate can be associated with the changes in the density of emitting Si-QDs, since, both, PL intensity and Si-QD density follow the similar trend of increasing when the NH_3 flow rate increases up to 200 scccm, and then they decrease for an NH_3 flow rate of 300 sccm. The PL spectrum of a film deposited at a NH_3 flow rate of 500 sccm was also included in Fig. 3 only to show that in this case the PL intensity decreases significantly due to the lower density of emitting Si-QDs in this film, in spite that this sample is much more thicker ($d \approx 375$ nm).

In order to carry out a more detailed analysis of the origin of the changes in the PL and the mechanisms of excitation–emission of light in these films, the optical absorbance of the films was plotted along with the normalized PL in Fig. 4, as a function of the photon energy. A small absorption band with a maximum

between 2 and 3 eV is observed in the absorbance curves of Fig. 4. Since this absorption band overlaps with the PL band, we can infer that it originated from interband optical transitions in the Si-QDs, where an electron jumps from the valence band (VB) to the conduction band (CB) of the Si-QDs by absorbing a photon. Two optical absorption edges are also observed in the absorbance spectra of all the samples, which shift toward higher energies (blue-shift) when the Si-QDs size decreases (by increasing the NH_3 flow rate). A large Stokes shift ($\sim$0.7–0.8 eV) between the first absorption edge and the emission peak, is also observed for all the samples.

In order to measure the energy of the two optical absorption edges, and since the SiN_x:Cl films are amorphous, we used the well-known Tauc plots, $(\alpha h\nu)^{1/2}$ vs $h\nu$, of Fig. 5, and extrapolate to zero ordinate each of the two straight lines fitted for each Tauc plot. Table 1 shows the energies of the two absorption edges measured for each sample. As can be seen from the data of this table, the energy of the first and second absorption edges increase from 3.0 to 3.5 eV and from 3.8 to 4.5 eV, respectively, as the NH_3 flow rate increases. The energies of the absorption edge 2 (E_{edge2}) can be associated with the band gap energy ($E_{g'}=E_{c'}-E_{v'}$) of the silicon-rich silicon nitride (SiN_x:Cl) matrix of the films. The increase of the band gap energy of the SiN_x:Cl matrix, from 3.8 to 4.5 eV, as the NH_3 flow rate increases from 50 sccm to 300 sccm is quite expected, since this increase changes the composition of the films toward stoichiometric silicon nitride (N/Si=1.33) which has a band gap of $\sim$5 eV.

Based on these data and since the energies of the PL peaks can be directly associated with the band gap energy ($E_g=E_c-E_v$) of the Si-QDs, we built the simplified energy bands diagram depicted in Fig. 6 in order to model the electronic structure of our nanostructured films, and the excitation–emission mechanisms. As can be seen in the energy band diagram of Fig. 6, we have added two energy band tails, below the CB and above the VB of the SiN_x:Cl matrix, which are well known to appear in amorphous silicon nitride films [23,24]. As it has been shown recently from PL measurements at cryogenic temperatures on a-SiN:H films, the width ($\Delta E=\Delta E_C=\Delta E_V$) of both sub-gap absorption tails is almost the same and increases with the NH_3/SiH_4 ratio of the reacting gases used for depositing the film, and is as high as ΔE=0.35 eV for a ratio of 9 [24]. It is worth to mention that the existence of a band tail gap ($E_{gtail}=E_{04}-2\Delta E$) was fundamental in that work (as well for this work) to explain why the PL of a-SiN:H films with optical gaps as high as 4.8 eV, can be excited with photons with energy of 3.81 eV from a He–Cd laser [24].

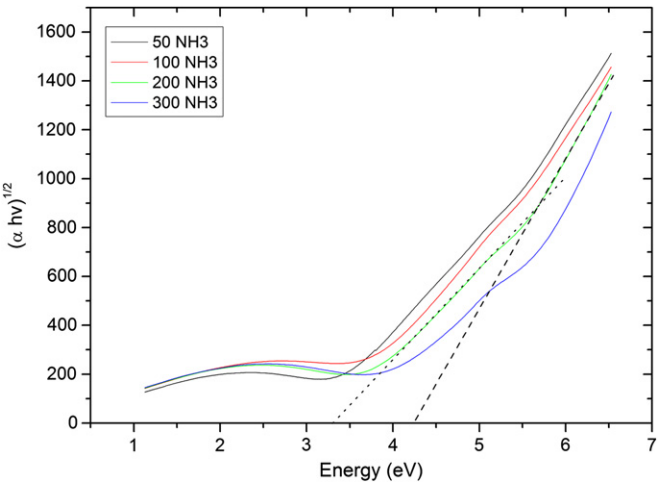

Fig. 5. Tauc plots of SiN_x:Cl films with embedded Si-QDs.

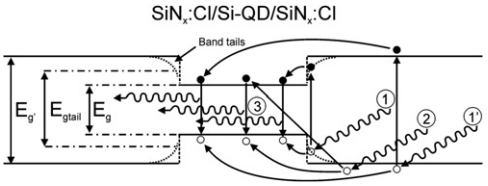

Fig. 6. Energy band diagram model proposed to explain the excitation–emission mechanism of Si-QDs embedded in SiN_x:Cl films.

In the case of our films, since the SiN_x:Cl matrix is amorphous, and the films were deposited using NH_3/SiH_2Cl_2 ratios of 10, 20, 40, 60, we can infer the existence of subgap optical absorption tails with a width (ΔE) of similar magnitude or higher. Based on this, the energy E_{edge1} of the optical absorption edge 1 calculated from the Tauc plots can be associated to absorption of photons which produce transitions of electrons from the VB energy tail to the CB energy tail of the SiN_x:Cl matrix. In other words, we can consider that for our SiN_x:Cl matrix $E_{gtail}=E_{g'}-2\Delta E=E_{edge1}$, which implies the reasonable values of ΔE listed in Table 1.

From these results and model we elucidate that the PL in these nanostructured films is generated by the following excitation–emission mechanisms: (I) photoexcitation with UV light of electrons from the VB tail to the CB tail (through E_{gtail}) or from the VB to the CB (through $E_{g'}$) of the SiN_x:Cl matrix (excitation processes 1 and 1′ in Fig. 6), (II) relaxation, diffusion and transfer of the photogenerated carriers (electrons and/or holes) from the SiN_x:Cl matrix to the Si-QDs (processes marked with curved arrows in Fig. 6), (III) electron–hole radiative recombination in the Si-QDs (processes 3 in Fig. 6). Assuming these excitation–emission mechanisms and that the level of the Fermi energy is the same and at the middle of the band gap of both the Si-QDs and the SiN_x:Cl matrix ($E_F=E_g/2=E_{g'}/2$), it is explained physically and quantitatively the large and approximately constant absorption/emission Stokes shift ($E_{edge1}-E_{PL}\sim$0.7–0.8 eV) for all the analyzed samples.

It is worth to mention that, interestingly, another possible photoexcitation mechanisms with 3.81 eV are from the VB of the SiN_x:Cl matrix to the CB of the Si-QDs (process 2 in Fig. 6), or even from the VB of the Si-QDs to the CB of the SiN_x:Cl matrix. However, since the volume of the SiN_x:Cl matrix is larger than the volume of Si-QDs, the photon has a higher probability to excite the electrons from the VB of the matrix than from VB of the Si QDs.

Finally, we used the formula; $E_{PL}=E_{SiBulk}+C/d^2$, where d is the dot diameter and E_{SiBulk}=1.16 eV, is the band gap for bulk crystalline silicon, in order to calculate the quantum confinement parameter C for our Si-QDs, and to compare with that reported by other authors [7,8,10]. As can be seen from Table 1 the values of the confined parameter increase from C=9.7 to 17.3 nm^2 eV, when d increases from 2.4 to 3.9 nm,. These results show that the quantum confinement effect for the larger Si-QDs, which tend to be more crystalline, is larger than that of smaller Si-QDs, and this trend is similar to that found previously [7,8,10]. The values of the confinement parameter obtained in this work are of the order of those reported previously for silicon nanocrystals embedded in hydrogenated silicon nitride films [8,10], and the discrepancies among them are well expected since this parameter is proportional to the reduced mass $1/m^*=1/m_e^*+1/m_h^*$, where m_e^* and m_h^* are the electron and hole effective masses, respectively, and in practice they must depend on the specific surface passivation and/or surrounding host of the Si-QDs, which in turn depend on the source gases and deposition conditions used to prepare these nanosctructured systems.

4. Conclusions

In summary we have investigated the PL and optical absorption properties of Si-QDs embedded in SiN_x:Cl nanometric thin films. We found that the PL of these Si-QDs can be blue-shifted in the visible range by reducing the size of the Si-QDs below the Bohr radius of excitons in confined silicon. Two optical absorption edges were observed in the absorption spectra of the films, which also blue-shift as the size of the Si-QDs decreases. From these experimental results we proposed a model for the excitation–emission mechanisms to explain the PL and the large absorption/emission Stokes shift of these nanostructured films. Although the blue-shift of the PL and absorption edges with the reduction of Si-QDs size can be explained in terms of quantum confinement effects, we conclude that the surface passivation of the Si-QDs also has influence on these effects.

Acknowledgment

The authors acknowledge the technical assistance of R. Hernández-Reyes, L. Huerta, J. Camacho and J.M. García–León and partial financial support from PAPIIT-UNAM under Project no. IN115711.

References

[1] F. Iacona, C. Bongiorno, C. Spinella, S. Boninelli, F. Priolo, J. Appl. Phys. 95 (2004) 3723.
[2] Z.X. Cao, R. Song, L.B. Ma, Y. Du, A.L. Ji, Y.Q. Wang, Nanotechnology 17 (2006) 2073.
[3] T. Nozaki, K. Sasaki, T. Ogino, D. Asahi, K. Okazaki, Nanotechnology 18 (2007) 235603.
[4] A. Marconi, A. Anopchenko, M. Wang, G. Pucker, P. Bellutti, L. Pavesi, Appl. Phys. Lett. 94 (2009) 221110.
[5] D. Das, A. Samanta, Nanotechnology 22 (2011) 055601.
[6] E.G. Barbagiovanni, L.V. Goncharova, P.J. Simpson, Phys. Rev. B 83 (2011) 035112.
[7] N.-M. Park, C.-J. Choi, T.-Y. Seong, S.-J. Park, Phys. Rev. Lett. 86 (2001) 1355.
[8] T.-Y. Kim, N.-M. Park, K.-H. Kim, G.Y. Sung, Y.-W. Ok, T.-Y. Seong, C.-J. Choi, Appl. Phys. Lett. 85 (2004) 5355.
[9] B.-H. Kim, C.-H. Cho, T.-W. Kim, N.-M. Park, G.Y. Sung, S.-J. Park, Appl. Phys. Lett. 86 (2005) 091908.
[10] T.-W. Kim, C.-H. Cho, B.-H. Kim, S.-J. Park, Appl. Phys. Lett. 88 (2006) 123102.
[11] L.D. Dal Negro, J.H. Yi, J. Michel, L.C. Kimerling, S. Hamel, A. Williamson, G. Galli, IEEE J. Sel. Top. Quantum Electron. 12 (2006) 1628.
[12] J.H.Y.L. Dal Negro, L.C. Kimerling, S. Hamel, A. Williamson, G. Galli, Appl. Phys. Lett. 88 (2006) 183103.
[13] A. Benami, G. Santana, A. Ortiz, A. Ponce, D. Romeu, J. Aguilar-Hernández, G. Contreras-Puente, J.C. Alonso, Nanotechnology 18 (2007) 155704.
[14] H.L. Hao, L.K. Wu, W.Z. Shen, Appl. Phys. Lett. 92 (2008) 121922.
[15] A. López-Suárez, J. Fandiño, B.M. Monroy, G. Santana, J.C. Alonso, Physica E: Low-dimensional Systems and Nanostructures 40 (2008) 3141.
[16] J.C. Alonso, G. Santana, A. Benami, B.M. Monroy, Luminescent Silicon Nanoclusters in SiNx Thin Layers, in: N.H.S. (Ed.), Encyclopedia of Nanoscience and NanotechnologyAmerican Scientific Publishers, 2011, pp. 1–31. ISBN: 1-58883-165-5.
[17] J. Wang, V. Suendo, A. Abramov, L. Yu, P. Roca i Cabarrocas, Appl. Phys. Lett. 97 (2010) 221113.
[18] G. Santana, B.M. Monroy, A. Ortiz, L. Huerta, J.C. Alonso, J. Fandiño, J. Aguilar-Hernández, E. Hoyos, F. Cruz-Gandarilla, G. Contreras-Puentes, Appl. Phys. Lett. 88 (2006) 041916.
[19] S. Godefroo, M. Hayne, M. Jivanescu, A. Stesmans, M. Zacharias, O.I. Lebedev, G. Van Tendeloo, V.V. Moshchalkov, Nat. Nanotechnology 3 (2008) 174.
[20] J.C.A. Ana Martínez, Luis.E. Sansores, Roberto Salcedo, J. Phys. Chem. C 114 (2010) 12427.
[21] Y. Ma, X. Chen, X. Pi, D. Yang, J. Phys. Chem. C 115 (2011) 12822.
[22] P.F. Trwoga, A.J. Kenyon, C.W. Pitt, J. Appl. Phys. 83 (1998) 3789.
[23] H. Kato, N. Kashio, Y. Ohki, K.S. Seol, T. Noma, J. Appl. Phys. 93 (2003) 239.
[24] M. Anutgan, T.A. Anutgan, I. Atilgan, B. Katircioglu, J. Lumin. 131 (2011) 1305.